Available online at www.sciencedirect.com
SCIENCE DIRECT®
International Journal of Heat and Mass Transfer 49 (2006) 3538–3546
International Journal of HEAT and MASS TRANSFER
www.elsevier.com/locate/ijhmt

Microtube liquid single-phase heat transfer in laminar flow

G.P. Celata [a,*], M. Cumo [b], V. Marconi [a], S.J. McPhail [a], G. Zummo [a]

[a] ENEA, Institute for Thermal Fluid Dynamics, Universita degli Studi di Bologna, Via Anguillarese 301, 00060 S.M. Galeria, Rome, Italy
[b] University of Rome 'La Sapienza', Corso Vittorio Emanuele II 244, Rome

Received 3 December 2005
Available online 11 May 2006

Abstract

One of the main applications of microscale flow is miniature, high-efficiency heat transfer. The most simple and immediate solution to the problem of concentrated heat exchange is the use of small diameter channels with single-phase water flow, but there is a lack of publicised knowledge about the heat transfer performance in these conditions. In this article, an experimental investigation is reported to accurately characterize the diabatic behaviour of single-phase laminar flow in circular microducts, ranging in diameter from 528 down to 120 μm. The experiments on a capillary of 50 μm ID proved upon analysis to be unaccountable due to the intrinsic error contained in the set-up, which is tied to the large inertia of the pipe wall, etc. in proportion to the small passage of flow at this diameter. The vacuum environment in which experiments were carried out ensured a test section free of convective losses, so that measurements are provided as precise as possible within the geometry of the microchannel. The possible occurrence of scaling effects such as axial conduction in the walls, viscous heating of the fluid and thermal entrance length effects was studied and criteria were established which have been validated by the measurements. Results show a *decrease* of Nusselt number with decreasing diameter, an axial dependence that is linked to thermal entrance effects and a dependence of the Nusselt number also on Reynolds number, whence the large conductive losses from the test section can be deduced, not necessarily restricted to axial redistribution of the heat flux in the wall only.

1. Introduction

The miniaturization of many appliances in biomedic, chemical and computer technology has brought with it increased demands for space-efficient high-performance heat dissipation and catalytic devices. Though much research on microscale level has already been done in recent years in the relevant fields, especially as regards hydrodynamic and heat transfer characterization, there is still much diversion of results to be discerned in the various experimental and numerical reports. The diversion occurs in different contexts: fluid drag of laminar, transient and turbulent single-phase flows, heat transfer of liquid and gas flows, and two-phase flow in adiabatic and heated microchannels; each with a vast class of problems relating to fluid type, phase or compressibility, channel shape and aspect ratio, surface properties and diabatic conditions.

Little work has been done on single-phase (liquid) heat transfer in micropipes. The most updated state-of-the-art review has been prepared by Palm [1] and by Palm and Peng [2]. Other authors proposed interesting reviews on single-phase (liquid) heat transfer in micropipes and/or microchannels, Obot [3], Rostami et al. [4], Morini [5], and Hetsroni et al. [6]. The most recent and interesting experiments have been carried out by Celata et al. [7], Bucci et al. [8], Lelea et al. [9], and Yen et al. [10].

In the experimental and theoretical investigations done over the past years, a number of contradictory conclusions have been drawn, but most inconsistencies prove to be originated by the difficulty of experimental conditions and high sensitivity of models to measurement errors. Knowledge of the field, in fact, tends towards an affirmation of conventional, "macro-scale" theory as accuracies improve. Nevertheless, more data and experience are required to map the influence of the particular characteristics of microscale flow correctly, and to establish the limits and criteria at which certain, purely microdimensional phenomena become

* Corresponding author. Tel.: +39 6 30483905; fax: +39 6 30483926.
E-mail address: celata@casaccia.enea.it (G.P. Celata).

0017-9310/$ - see front matter © 2006 Elsevier Ltd. All rights reserved.
doi:10.1016/j.ijheatmasstransfer.2006.03.004

Nomenclature

A	area, m^2
Br	Brinkman number, $\mu U^2/q'_w$
c_p	fluid specific heat, J/kg K
D	tube diameter, m
e_y	absolute error of parameter y
f	Darcy friction factor, –
Gz	Graetz number, Eq. (1)
h	heat transfer coefficient, W/m^2 K
k	thermal conductivity, W/m K
K	geometry-dependant constants in Eq. (2)
L	channel length, m
p	pressure of fluid in duct, Pa
p^*	dimensionless pressure defined in Eq. (3)
Pr	Prandtl number, $c_p\mu/\kappa$
q'	linear heat flux, W/m
q''	heat flux, W/m^2
Re	Reynolds number, $\rho UD/\mu$
T	temperature, K
U	fluid average velocity, m/s
x	axial co-ordinate, m

Greek symbols

Γ	mass flow, kg/s
ε	body emissivity
κ	proportion of viscous heating to total temperature rise
μ	dynamic viscosity, Pa s
ρ	fluid density, kg/m^3
σ	Stefan–Boltzmann constant, 5.669×10^{-8} W/m^2 K^4
Φ^*	dimensionless viscous-energy-dissipation function
Ω	cross-sectional area, m^2
Ω^*	dimensionless cross-sectional area, Ω/D_h^2

Subscripts

b	bulk
e	external
exp	experimental
f	fluid
ht	heated
i	inner, internal
o	outer
q	pertains to the heat input
rad	radiative
v	pertains to viscous dissipation
w	wall

important. In [13], the influence of viscous dissipation is analysed – a good example of such a *scaling effect*. Below a certain characteristic dimension of the system, this phenomenon – which is present but undetectable for larger geometries – manifests itself, and must be taken into consideration. In the case of the effect of viscous dissipation, this could be used proficiently to deduce the friction factor of the channel under investigation – a valuable alternative to a pressure-drop-based determination.

This paper deals with the characterization of forced convection heat transfer in microtubes, and introduces some of the difficulties caused by other effects linked to microscopic channel sizes: the thermal entrance length and conjugate heat transfer.

2. Theoretical background

2.1. Thermal entrance length

The thermal entrance length is a transitory region where flow at uniform temperature develops under influence of uniformly heated walls to a steady-state profile of temperature that is dependent on fluid velocity and conductivity. Just like it is the case for the physics of *flow* in the *hydrodynamic* entrance region, the mechanism of *heat transfer* is rather different in the *thermal* entrance length (see Fig. 1).

Fluid enters the heated section of a pipe with a uniform temperature (in our case, the velocity profile is already fully developed at this stage), and as the heat input is absorbed, the temperature of the fluid at the wall starts to rise. Through conduction across the fluid layers of the laminar flow, the temperature profile then develops over the entire cross-section. The superposition of the convective force then creates the thermal developing length (from $x = 0$ to $x = x_T$ in Fig. 1). Whether a heated flow has reached this semi-steady thermal state (the *bulk* temperature will of course be increasing steadily), can be deduced from the value of the Graetz number:

$$Gz = Re\,Pr\frac{D}{x} \tag{1}$$

A thermally fully developed profile is achieved when $Gz < 10$, so the longer the distance x along the channel axis and the less force of convection Re, the more chance there is of obtaining a thermally fully developed profile.

The effect of a thermal entrance region is to increase the Nusselt number compared to that of the thermally fully developed region. The generalized Hausen correlation describes the *mean* Nusselt number as the sum of two terms: a fully developed value of the Nusselt number, and a term taking into account the effects of the thermal entrance region:

$$\langle Nu\rangle = Nu_\infty + K_1\frac{Gz}{(1 + K_2 Gz^b)} \tag{2}$$

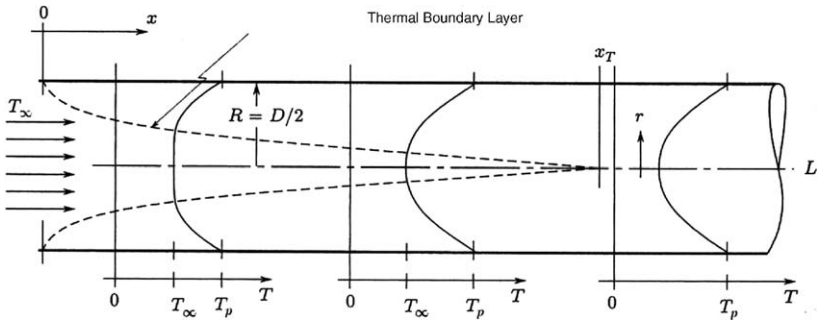

Fig. 1. Thermally developing flow.

Here the Graetz number is taken over the entire length of channel, and in the case of constant wall heat flux and fully developed velocity profile, for circular ducts: $K_1 = 0.023$, $K_2 = 0.0012$ and $b = 1$ [11].

2.2. Axial conduction in the walls

For low values of the Reynolds number, the mean value of the Nusselt number coincides with the fully developed value, because the entrance region is very short and the effects of the viscous dissipation are not important in this regime of flow. On the contrary, at low Reynolds numbers the effects of *conjugate* heat transfer on the mean value of the Nusselt number may become very important because conduction along the channel walls becomes a competitive mechanism of heat transfer with respect to internal convection. Maranzana et al. [12] evidenced through numerical simulation that when the effects of conjugate heat transfer are predominant, the temperature distribution along the microchannel is not linear at all (see Fig. 2).

The *mean* heat transfer coefficient, calculated with average temperatures, if one were to assume a linear fluid temperature distribution (the case of perfectly uniform wall heat flux):

$$\langle h \rangle = \frac{q''}{(\overline{T}_w - \overline{T}_f)} \tag{3}$$

is underestimated then, because the mean value of the bulk temperature along the microchannel, $\overline{T}_f$, is underestimated. This is also an explanation for the dependence of the Nusselt number on the Reynolds number which is found in experiments, as this effect of underestimation will become less as the convective term of heat transfer ($\sim Re$) increases with respect to the conductive term in the channel wall. The temperature distribution along the tube axis will then approach a linear tendency (although the effects of thermal development would increase, see Eq. (3)).

Maranzana et al. [12] defined a criterion for the region of significance of axial conduction in the walls in the (conjugated) heat transfer problem, used also by Morini [13]. For a circular tube it calculates as

$$\left(\frac{k_w}{k_f}\right)\left(\frac{D_o^2 - D_i^2}{D_i L}\right)\frac{1}{Re\,Pr} > 10^{-2} \tag{4}$$

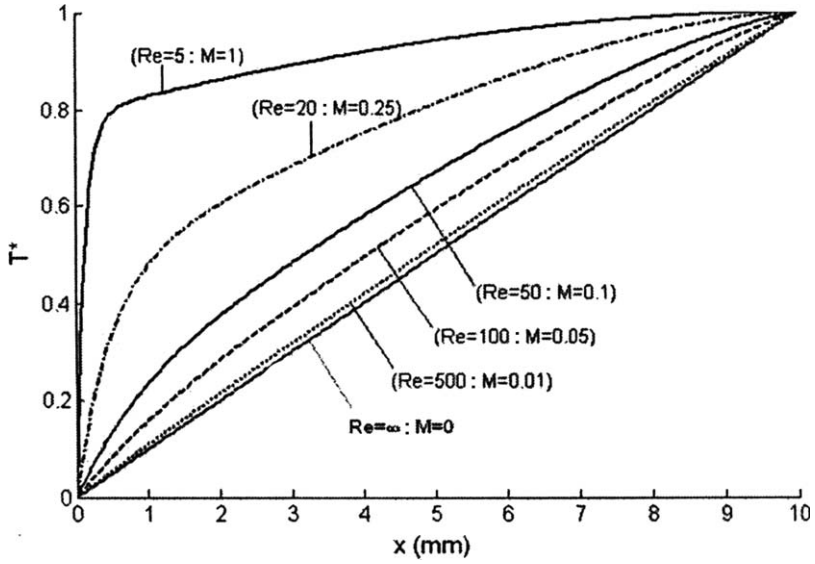

Fig. 2. Normalized bulk temperature along the axis for uniform heat flux at several Reynolds and M numbers [12].

The dimensionless quantity at the l.h.s. of Eq. (7), named M by the former cited authors, allows the comparison of heat transfer by axial conduction in the wall with the convective heat transfer in the flow.

2.3. Viscous heating

The influence of viscous heating in microchannels is pointed out and qualified in another article by the same authors [14] using the same experimental set-up. Below a certain diameter of channel, the viscous deformation of the laminar flow is such that heating of the fluid along the axis starts to become significant – an effect which is almost always negligible in conventional, macro-scale applications. Therefore, in a diabatic microsystem, this phenomenon needs to be taken into account, so that discrimination can be made between the effects of heat *input* and of viscotic heat *generation*.

Derived from the same set of equations as related in [14], it is possible to calculate the ratio between the fluid temperature rise related to viscous heating and the rise related to the heat flux at the walls as a function of the Brinkman number (Br) and of the Poiseuille number (fRe, equal to 64 for circular channels and the Darcy–Weisbach definition for the friction factor):

$$\kappa = \frac{\Delta T_{f\_v}}{\Delta T_{f\_q}} = 1/2 Br \Omega^* fRe \tag{5}$$

Here Ω^* is the dimensionless cross-sectional area, and κ can be taken as, say, 5% for the viscous heating to be considered negligible.

3. Experimental procedure

The test rig used for validation of the above effects is schematised in Fig. 3.

Experiments are carried out using demineralised water, which is degassed by passing through a very small, but continuous quantity of Helium. Being insoluble in water, an atmosphere of only Helium is created above the liquid level, so that all dissolved gases are driven out by their respective partial pressures in the water. A gear pump is used to drive the flow, which passes through a 10 μm filter and is controlled with a microvalve regulator, before entering the test section.

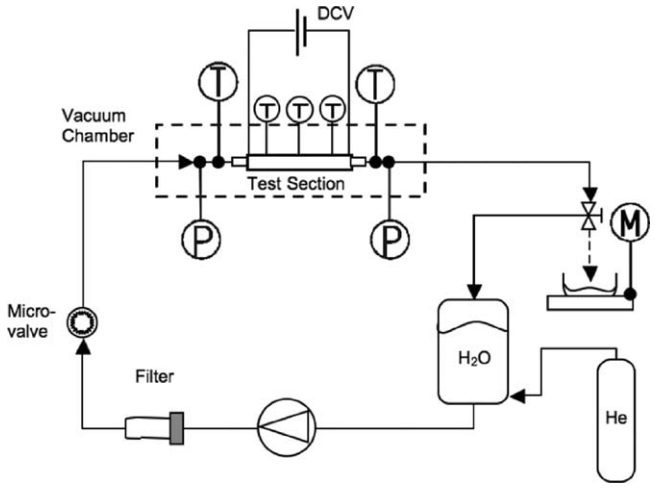

Fig. 3. Test rig for circular channel heat transfer experiments.

The microtube under investigation is mounted inside a stainless steel capsule (see Fig. 4) which is sucked vacuum by a turbo-molecular vacuum pump (Alcatel ATS-100) to create an environment free of natural convection. To this effect, the level of vacuum must be less than 10^{-3} mbar. The level obtained in our set-up is 2×10^{-4} mbar (Edwards Penning Gauge Model 6), so that we can consider the heat loss to the surroundings through convection inexistent.

The heat loss due to radiation is evaluated by considering the formula for two concentric cylindrical surfaces, simplified for the limiting case where the surface of the internal body (OD of the test section is 0.9 mm) is much smaller than the external, concave surface (ID of the vacuum chamber is 100 mm):

$$q'_{rad} L = \sigma A_i \varepsilon_i (T_i^4 - T_e^4) \tag{6}$$

The entity of this loss is of the order of 0.01% in the case of the highest measured temperature difference between the two bodies, and thus considered negligible.

The only heat loss term of any importance would then be conduction through connecting wires, leads and tubing. The entity of this loss is difficultly quantifiable, inasmuch as it depends on the mass, conductivity and temperature of the various materials in contact with the test section. It is expected to be of influence, however, only in the case of extremely low fluid flow and high heat input.

A 250 μm K-type thermocouple measures the fluid temperature on entrance into the test section, and pressure transducers on either side of the microtube investigated allow the pressure drop over the channel to be established (Druck PTX100/IS, 0–35 bar; Transamerica 0–160 bar); also a differential manometer is mounted parallel to the transducers for extra precise differential pressure measurements.

A constant power DC supply is used to heat the test section, which is fitted with Gas Chromatography fittings (Upchurch Scientific) resistant to high temperature and pressure.

At the outlet of the channel, a 50 μm K-Type thermocouple is made to be inserted inside the (Near-Zero) dead volume of the fitting so that the fluid exit temperature (a critical quantity) is measured as closely as possible. The mass flow rate is measured with a high precision scale.

3.1. Tubes tested

The capillaries under consideration in this study (see e.g. Fig. 5a and b) are vitreous and therefore have extremely smooth inner surfaces. Glass tubes of varying inner diameter, manufactured in-house, were coated with a uniform, 100 nm layer of chromium–molybdenum or chromium–gold (through sputtering technology) to materialise 35 mm

Fig. 4. Close-up of vacuum chamber and flange with mounted test section (circled), thermocouples and pressure ducts.

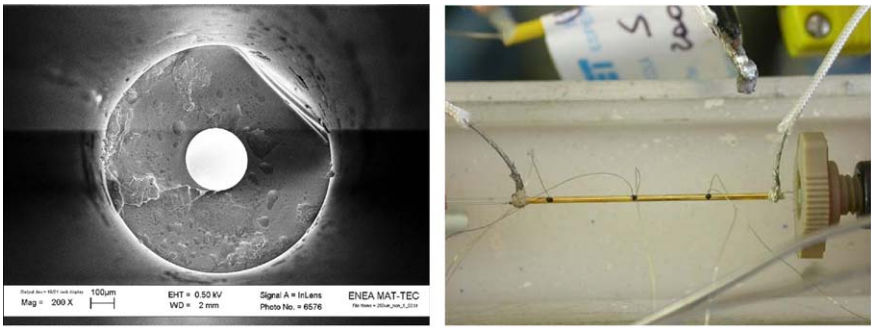

Fig. 5. Capillaries studied: SEM image of cross-section (a) and fitted with thermocouples attached to channel wall (b).

of heating length (see Fig. 5b). The outer diameter of these capillaries is practically constant (~0.9 mm).

To determine the local heat transfer coefficient, it is necessary to know the *inner* wall temperature at that location, but as it is impossible to measure this value directly, due to the geometry and material of the channels, the *outer* wall temperature is measured instead. This is achieved by attaching 50 μm K-type thermocouple wires to the outer wall with cyanacrylic adhesive at first and subsequently fixing them with a non-conductive epoxy resin (see Fig. 5b). This ensures in addition to a quick and reliable response, that there is no electrical conductance to disturb the temperature measurement. We can then deduce the inner wall temperature using Fourier's conduction law across a cylindrical surface (second term in Eq. (7)).

3.2. Uncertainty analysis

In order to evaluate the influence of experimental parameters on the measurement of the variable of interest, it is convenient to perform an uncertainty analysis. The local heat transfer coefficient, expressed in terms of measurable quantities only, is as follows:

$$h(x) = \left[\frac{\pi D_i L_{ht}(T_{w\_o}(x) - T_f(x))}{\Gamma c_p \Delta T_f} - \frac{D_i}{2k_w}\ln\left(\frac{D_o}{D_i}\right)\right]^{-1} \qquad (7)$$

The heat flux is evaluated from the enthalpy rise of the fluid ($\Gamma c_p \Delta T_f$). For the determination of the local fluid temperature $T_f(x)$ a linear temperature rise is assumed along the heated length of tube. The second term on the r.h.s. represents the temperature distribution due to conduction from the metal coating across the wall thickness to the fluid interface.

Following classic methodology set out in e.g. [15], one arrives at a definition of the relative experimental error as a function of the uncertainty on each of the measured quantities. (Due to the intricate composition of the equation that results, it is not reported here.)

Analyzing Eq. (7) it can be noticed that there is an instability in the description of h where the two terms in the square brackets become equal. In certain experimental conditions the combination of these variables may be very close to this singularity, in which case there is a high degree of sensitivity to the measurement error. This is liable to produce some unrealistic elaborations, as will be seen from some of the results presented in the next chapter.

4. Results and discussion

The matrix of experiments eventually is as represented in Table 1. The results will be presented in the form of local Nusselt number vs. Reynolds number graphs for each

Table 1
Experimental conditions

D_i (μm)	D_o (μm)	e_{D_i} (μm)	L (mm)	L_{HT} (mm)	$\langle Re \rangle$	$\langle Gz \rangle$	$M \times 10^6$	κ (%)
528	859	3.9	79.0	36.8	50–2775	9–233	3–70	0.001–0.1
325	909	4.7	79.5	37.6	274–2304	10–117	8–95	0.03–1.2
259	951	4.4	82.1	36.4	105–2576	3.5–103	12–330	0.06–1.4
120	804	2.4	65.4	35.4	279–3138	6–58	17–170	0.1–10
50	363	1.3	66.0	34.2	114–1450	1–13	32–428	0.6–35

channel diameter, at three axial locations and for two ranges of heat input (for the 50 μm ID tube: two axial locations and three heat flux values). The reference value of the Nusselt number for thermally fully developed flow is always given as a reference.

The axial locations are distributed as follows:

$$x(1) \approx 0.3L_{ht}, \quad x(2) \approx 0.6L_{ht}, \quad x(3) \approx 0.9L_{ht}.$$

The heat absorbed is divided in three ranges:

$$50 < q''\mathrm{I} < 100\ \mathrm{kW/m^2}$$

$$120 < q''\mathrm{II} < 180\ \mathrm{kW/m^2}$$

$$380 < q''\mathrm{III} < 450\ \mathrm{kW/m^2}.$$

To conclude, an overview plot of *global* Nusselt vs. *global* Reynolds numbers is presented for all diameters, with a reference correlation included for comparison (Eq. (2)).

To begin with the largest diameter (528 μm), the results depicted in Fig. 6 are clearly indicative of thermally developing flow. There is a considerable axial dependence of the heat transfer coefficient, with higher Nusselt numbers nearer to the channel inlet. In fact, as is known from classical theory, the less thermal development, the stronger the drive for heat exchange (the factor is quantified in [16] as an *incremental heat transfer number*). Eq. (2) also expresses this dependence for the *global* Nusselt number, of which we will see the positive agreement later in Fig. 10. The advent of turbulence and its increased heat transfer efficiency can be individuated where the curves turn sharply upwards at $Re \approx 2300$.

As we can see from the table of experimental conditions, at 528 μm ID (due to the relatively short length of heated tube) the flow is nearly always in thermal development ($Gz > 10$). Therefore only nearest to the exit ($x(3)$ in the figure) and at low Reynolds numbers do we approach the thermally developed state corresponding to the constant value for the Nusselt number, 4.36.

In Fig. 7 above, the experimental data of the 325 μm ID tube can be seen. We notice with respect to the 528 μm ID duct a *decrease* of the local Nusselt numbers at equal Reynolds numbers and a *weaker* axial differentiation. Also, a positive dependence on the heat input is now discernable, which increases at higher Reynolds numbers.

Decreasing the inner diameter further (259 μm, see Fig. 8), we find an *ulterior decrease* in Nusselt number. The dependence on the Reynolds number diminishes slightly (a flatter profile) as well as the axial dependence (local values closer together).

The trend that was already observed is continued for the 120 μm tube as regards the *lowering* of the local Nusselt numbers and the decrease in axial dependence (Fig. 9). In fact, at this diameter the heated length is relatively much larger so that the flow reaches thermal development well inside the test section and no more axial dependence is expected. We can see from Table 1 that the Graetz number is still mainly above 10, but compared to the larger tubes the order of magnitude is distinctly lower.

There is still a distinct dependence on Reynolds number present, however. This could be due – at this proportion of

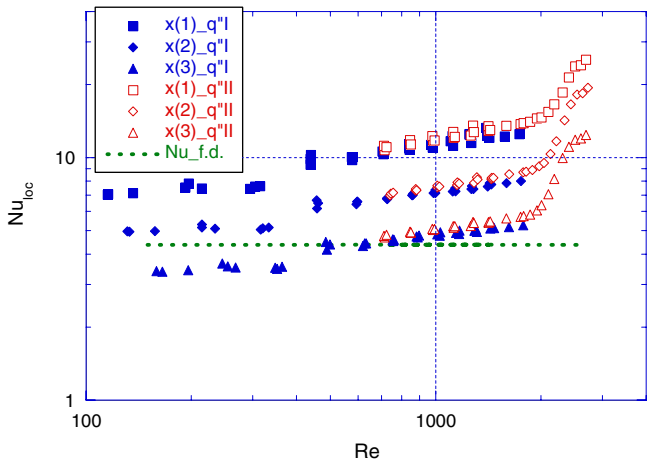

Fig. 6. 528 μm ID tube: local Nusselt vs. Reynolds numbers at three axial locations; two ranges of heat input.

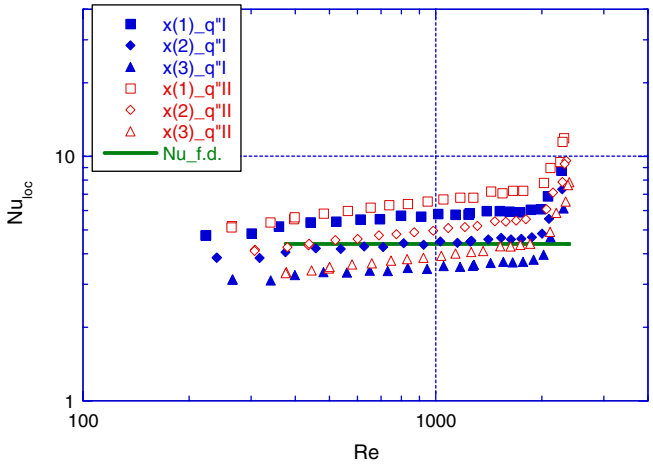

Fig. 7. 325 μm ID tube: local Nusselt vs. Reynolds numbers at three axial locations; two ranges of heat input.

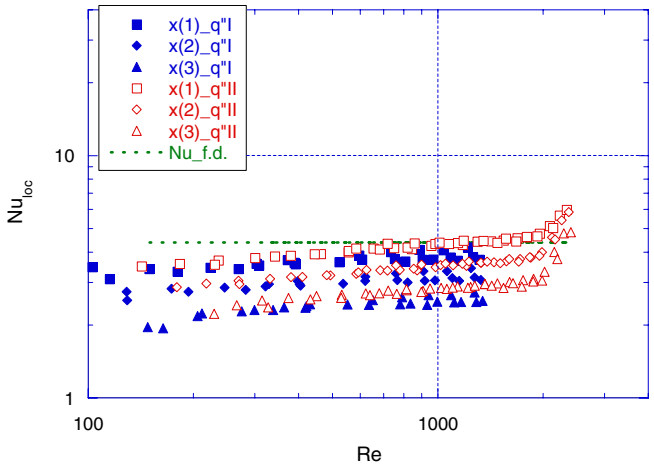

Fig. 8. 259 μm ID tube: local Nusselt vs. Reynolds numbers at three axial locations; two ranges of heat input.

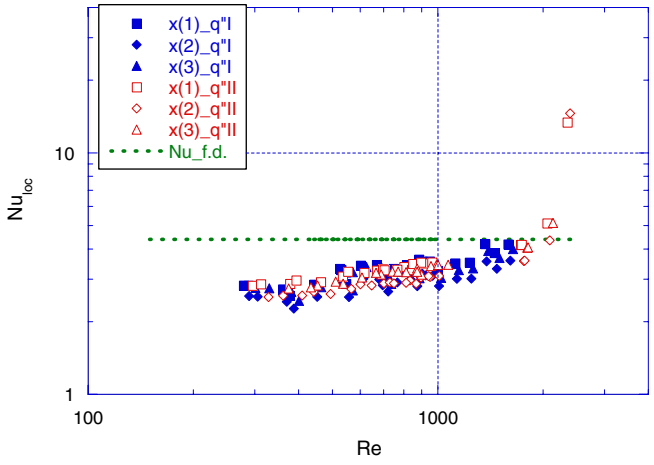

Fig. 9. 120 μm ID tube: local Nusselt vs. Reynolds numbers at three axial locations; two ranges of heat input.

inner and outer diameter – to an insipience of the phenomenon of axial conduction in the walls and of other materials attached to the test section. At very small diameters, the mass flow of fluid becomes itself extremely reduced compared to the mass of connected auxiliaries. Thus, to bring the entire system to a stable temperature means to distribute excessively the little heat convected by the fluid so that large losses and long settling times are the consequence. In fact, if we look at the criterion given for the M number, we find that the values of this number for all experiments carried out here (see Table 1) are well below the limit suggested for the occurrence of significant axial conduction. This seems to point at disturbances (heat sinks) that lie outside the system boundary of the channel strictly, like e.g. thermocouples, fittings and connected tubing.

Also from Table 1 we see that the viscous heating of the fluid becomes relevant at these diameters ($\kappa > 1\%$). This means that at higher Reynolds numbers not all of the temperature rise of the fluid is energy absorbed from the heat flux at the walls, but that some heat has been "autonomously" generated. Thus, the parameter of heat transfer, Nu, is overestimated where this is a relevant effect (smallest D_i, highest Re).

We can valuably summarize these observations by comparing the *global* Nusselt numbers of the various diameters. This means that *average* values of the fluid and wall temperatures are used to determine the heat transfer efficiency of the tube in consideration. The graph is shown in Fig. 10.

As was discussed earlier, the surprising effect of a *decrease* in Nusselt number with smaller diameters is apparent. It should be specified that the *heat transfer coefficient*, h, does increase, but not as much as the reduction in diameter, so that the dimensionless parameter Nu shows a net diminution. In fact, in comparison to the description of the global Nusselt number in laminar flow of Eq. (2), only the largest channel (528 μm ID) fits well (the solid line). For smaller diameters, conventional theory does predict a straightening of the curve as a function of the Reynolds number, but the limit value of 4.36 is maintained, and no lowering of the overall heat transfer efficiency was expected.

There is a slight dependence on heat input visible, especially at the intermediate diameters. For large ducts this is not the case, but at smaller diameters the radial temperature profile becomes more deformed due to the higher fluid velocity, so that the temperature-dependant physical properties of the fluid start to become influential. Reducing the diameter further, probably conduction to auxiliary connections starts to play an important role in equating and redistributing the heat flux imposed at the walls, as well as a superpositioning of axial temperature gradients (conjugate heat transfer). It should be noted however, that according to the criterion mentioned in the relative paragraph, the values of the M number in our experiments are always well below the stated limit for significance of this effect (see Table 1).

The very sharp increase in the global Nusselt number at the insipience of turbulent flow, however, especially at the smallest diameter, seems to hint at a heat transfer behaviour

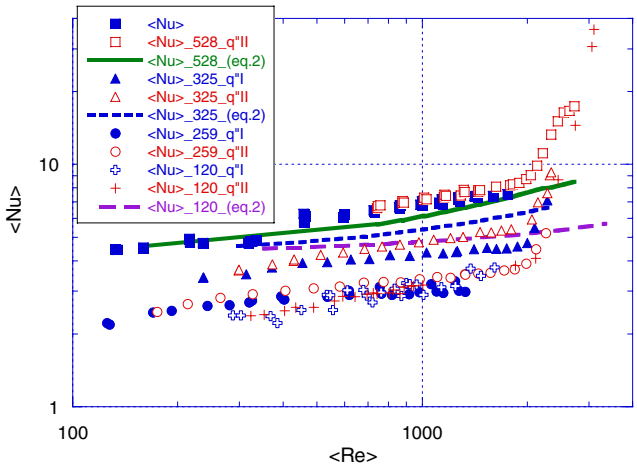

Fig. 10. Global Nusselt vs. global Reynolds numbers for four diameters and two heat input ranges; reference lines: Eq. (2).

that is much more efficient with respect to what is predicted for conventionally sized channels (e.g. Gnielinski correlation). The obvious difficulty is the enormous pressure requirements for these conditions of flow.

4.1. 50 μm Tube

Finally, it is interesting to share the experimental manifestation of the singularity in Eq. (7). The smallest capillary tested has an inner diameter of 50 μm and an outer diameter of around 363 μm. The results of the single-phase heat transfer experiments are shown in Fig. 11. For this tube, it was possible to study only two axial locations, but a third range of heat input was applied.

The anomaly is immediately apparent. A vertical asymptote can be observed for certain definite values of the Reynolds number, each corresponding to a different level of heat input or axial location. This is of course physically non-sense, but it shows very clearly how the experimental error can be of sudden extreme influence. At the various experimental conditions indicated by the asymptotes, the quantities of the conduction and convection term in Eq. (7) become equal and it is impossible to determine the conditions of heat transfer precisely (with the instruments available).

If we analyse the uncertainty more in detail around one of these experimental points, we can take into consideration the nine variables in Eq. (7) and plot their influence on the total experimental error at these conditions.

For example, around Reynolds number 700, heat input q''I (just after the asymptote), one of the datapoints has the following conditions:

$D_i = 50$ μm; $D_o = 363$ μm; $L_{ht} = 34$ mm;
$T_{w\_o} = 31.1$ °C; $T_f = 28.8$ °C; $\Gamma = 0.023$ g/s;
$\Delta T_f = 3$ K.

With constant values for c_p and k_w (4180 J/kgK and 1.38 W/mK respectively) the local Nusselt number calculates as −22, and the total experimental error shoots up from around 10% at more stable conditions to 80% with the above quantities for the variables plus their certified uncertainties (0.1 K on the thermocouple values, e.g.).

Let us observe the *fluid temperature rise*: by varying this value where the other parameters remain constant we get an idea of the instability of this experimental condition (see Fig. 12).

As we can see from the graph, there is a sharp peak in the total error on the heat transfer coefficient, just around the conditions we are working at ($\Delta T_f = 3$ K). The same effect is visible for each of the other variables analysed around this particular set of conditions (except D_o).

The relative contribution to the total experimental error of each of the variables at this condition (still with ΔT_f as the parameter that is varied) also shows this – purely conceptual – singularity (see Fig. 13).

It can be concluded that the experimental test rig is unfit to do experiments on this size of tube in its current

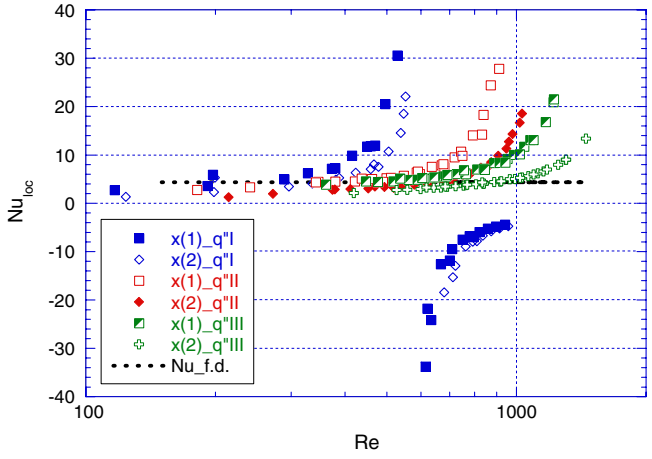

Fig. 11. 50 μm ID tube: local Nusselt vs. Reynolds numbers at two axial locations; three ranges of heat input.

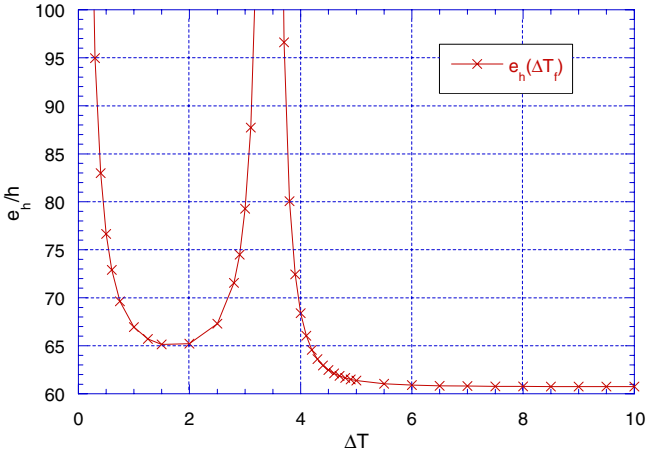

Fig. 12. Total experimental error for the 50 μm tube at one condition varying only the value of the fluid temperature rise along the test section.

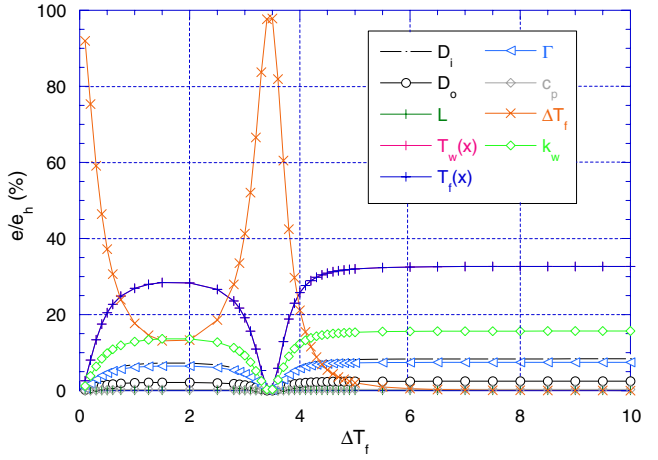

Fig. 13. Parameter contribution weight to total experimental error for the 50 μm tube at one condition varying only the value of the fluid temperature rise along the test section (ΔT).

configuration and with the available level of precision. This also illustrates the importance of effectuating a thorough error analysis *before* embarking on an extended program of laboratory effort.

5. Conclusions

An experimental validation has taken place of various single-phase heat transfer scaling effects that are of influence in microscale laminar flow. Smooth, circular channels were coated with a 100 nm layer of metal to provide an imposed, uniform heat flux at the walls, and fitted with thermocouples at three axial locations to estimate the local heat transfer coefficient for various conditions of flow. Four inner diameters were profitably studied: 528 μm, 325 μm, 259 μm and 120 μm. The largest diameter channel clearly exhibited heat transfer behaviour of thermally developing flow (increase of the Nusselt number compared to the fully developed value, more marked closer to the inlet). The smaller microtubes show progressively less evidence of flow in the course of thermal development (indicated especially by a reduced axial dependence of the Nusselt number): this is due to the higher length-to-diameter ratio of the smaller channels. An overall *decrease* in Nusselt number, for all Reynolds numbers up to transition to turbulence is the most remarkable find. Furthermore, the decrease in heat transfer performance with respect to the conventional value ($Nu = 4.36$) is more marked for decreasing Reynolds number. This is probably due to a heat loss term that has the same effects as axial wall conduction (an effect which should not be present for given experimental conditions according to Eq. (4)). In other words, the convective heat absorption of the fluid in the tube is not the dominant force any more (as for high values of the Reynolds (or Péclet) number), but is counterbalanced by a dissipation term that is unaccounted for. Neglecting this dissipation term causes the measured wall and fluid temperatures to point at worsened convective heat exchange. This dissipation term might be tied to peripheral conduction away from the test section, through attached wires for example. This effect is all the more significant as the passage of flow gets smaller and the mass flux diminishes. Further ascertainment is required.

For the smallest channel studied (50 μm ID), the sensitivity to measurement errors is so large that it is impossible to obtain a realistic estimate of the heat transfer coefficient. An accurate study of the material that composes any (single-phase) microheat-exchanger system is therefore recommended, as the masses and inertia of auxiliaries can have particularly disturbing effects on heat transfer performance.

Acknowledgments

The realization of this article is in great part fruit of the patient devotion of our tube doctor, Antonio Scotini. The financial support of the EU, through FP6 HMT-MIC, RTN Contract HPRN-CT-2002-00204 is gratefully acknowledged.

References

[1] B. Palm, Heat transfer in microchannels, Microscale Thermophys. Eng. 5 (2001) 155–175.
[2] B. Palm, X.F. Peng, Single-phase convective heat transfer, in: G.P. Celata (Ed.), Heat Transfer and Fluid Flow in Microchannels, Begell House, New York, 2004.
[3] N.T. Obot, Toward a better understanding of friction and heat/mass transfer in microchannels—a literature review, in: Proceedings of the International Conference on Heat Transfer and Transport Phenomena in Microscale, Banff, Canada, October 15–20, 2000.
[4] A.A. Rostami, N. Saniei, A.S. Mujumdar, Liquid flow and heat transfer in microchannels: a review, Int. J. Heat Technol. 18 (2) (2000) 59–68.
[5] G.L. Morini, Single-phase convective heat transfer in microchannels: a review of experimental results, Int. J. Thermal Sci. 43 (2004) 631–651.
[6] G. Hetsroni, Heat transfer in micro-channels: comparison of experiments with theory and numerical results, Int. J. Heat Mass Transfer (2005). Available from: <www.sciencedirect.com>.
[7] G.P. Celata, M. Cumo, M. Guglielmi, G. Zummo, Experimental investigation of hydraulic and single phase heat transfer in 0.130 μm capillary tube, Microscale Thermophys. Eng. 6 (2002) 85–97.
[8] A. Bucci, G.P. Celata, M. Cumo, E. Serra, G. Zummo, Water single-phase fluid flow and heat transfer in capillary tubes, Thermal Sci. Eng. 11 (6) (2003) 81–89.
[9] D. Lelea, S. Nishio, K. Takano, The experimental research on microtube heat transfer and fluid flow of distilled water, Int. J. Heat Mass Transfer 47 (2004) 2817–2830.
[10] T.H. Yen, N. Kasagi, Y. Suzuki, Forced convective boiling heat transfer in microtubes at low mass and heat fluxes, Int. J. Multiphase Flow 29 (2003) 1771–1792.
[11] W.M. Rohsenow, H.Y. Choi, Heat, Mass and Momentum Transfer, Prentice-Hall, 1961 (as cited in [13]).
[12] G. Maranzana, I. Perry, D. Maillet, Mini- and micro-channels: influence of axial conduction in the walls, Int. J. Heat Mass Transfer 47 (2004) 3993–4004.
[13] G.L. Morini, Viscous dissipation as scaling effect for liquid flows in microchannels, in: Proceedings of 3rd International Conference on Mini and Microchannels, Toronto, Ont., Canada, 2005.
[14] G.P. Celata, V. Marconi, G.L. Morini, S.J. McPhail, G. Zummo, Using viscous heating to determine the friction factor in microchannels—an experimental validation, ECI Conference on Microchannels, Ciocco, Italy, 2005.
[15] J.P. Holman, Experimental Methods for Engineers, McGraw-Hill, 1978.
[16] R.K. Shah, A.L. London, Laminar flow forced convection in ducts, in: T.F. Irvine, J.P. Hartnett (Eds.), Advances in Heat Transfer, Academic Press, New York, 1978.